CrossMark

RESEARCH PAPER

Uptake, delivery, and anticancer activity of thymoquinone nanoparticles in breast cancer cells

Isabelle Fakhoury · Walid Saad ·
Kamal Bouhadir · Peter Nygren ·
Regine Schneider-Stock · Hala Gali-Muhtasib

Abstract Thymoquinone (TQ) is a promising anti-cancer molecule but its development is hindered by its limited bioavailability. Drug encapsulation is commonly used to overcome low drug solubility, limited bioavailability, and nonspecific targeting. In this project, TQ nanoparticles (TQ-NP) were synthesized and characterized. The cytotoxicity of the NP was investigated in nontumorigenic MCF-10-A breast cells, while the uptake, distribution, as well as the anticancer potential were investigated in MCF-7 and MDA-MB-231 breast cancer cells. Flash Nanoprecipitation and dynamic light scattering coupled with scanning electron microscopy were used to prepare and characterize TQ-NP prior to measuring their anticancer potential by MTT assay. The uptake and subcellular intake of TQ-NP were evaluated by fluorometry and confocal microscopy. TQ-NP were stable with a hydrodynamic average diameter size around 100 nm. Entrapment efficiency and loading content of TQ-NP were high (around 80 and 50 %, respectively). In vitro, TQ-NP had equal or enhanced anticancer activity effects compared to TQ in MCF-7 and aggressive MDA-MB-231 breast cancer cells, respectively, with no significant cytotoxicity of the blank NP. In addition, TQ and TQ-NP were relatively nontoxic to MCF-10-A normal breast cells. TQ-NP uptake mechanism was both time and concentration

I. Fakhoury · H. Gali-Muhtasib (✉)
Department of Biology, American University of Beirut, Beirut, Lebanon
e-mail: amro@aub.edu.lb

W. Saad
Department of Chemical and Petroleum Engineering, American University of Beirut, Beirut, Lebanon

K. Bouhadir
Department of Chemistry, American University of Beirut, Beirut, Lebanon

P. Nygren
Department of Immunology, Genetics and Pathology, Experimental and Clinical Oncology, Uppsala University, Uppsala, Sweden

R. Schneider-Stock
Experimental Tumor Pathology, Institute for Pathology, University of Erlangen-Nuremberg, Erlangen, Germany

H. Gali-Muhtasib
Department of Anatomy, Cell Biology, Physiology, Faculty of Medicine, American University of Beirut, Beirut, Lebanon

dependent. Treatment with inhibitors of endocytosis suggested the involvement of caveolin in TQ-NP uptake. This was further confirmed by subcellular localization findings showing the colocalization of TQ-NP with caveolin and transferrin as well as with the early and late markers of endocytosis. Altogether, the results describe an approach for the enhancement of TQ anticancer activity and uncover the mechanisms behind cell-TQ-NP interaction.

Keywords Thymoquinone · Breast cancer · Nanoparticles · Uptake · Endocytosis

Introduction

Thymoquinone (TQ), isolated 50 years ago from *Nigella sativa* black seed oil, has shown promising biological activities including antioxidant, anti-inflammatory, and anticancer effects. The potential of translating TQ to the clinic is supported by evidence that it inhibits cancer onset, survival, and progression and protects major organs from chemotherapy toxicity (Schneider-Stock et al. 2014). However, TQ's hydrophobic nature, poor solubility, and low bioavailability make its translation to the clinic challenging. Nanoparticle (NP) encapsulation of poorly soluble drugs is commonly used for increasing drug dissolution and bioavailability. Nanoparticle drug delivery systems have made significant clinical impact by improving the pharmaceutical efficacy and dosing of a variety of already approved drugs (Lammers et al. 2012). Nanoparticle formulation is a rapidly progressing field in cancer treatment (Brannon-Peppas and Blanchette 2004; Lopez-Davila et al. 2012; Zamboni et al. 2012) as it can enhance drug accumulation in tumors, prevent rapid drug metabolism and lysosomal degradation, and lower the exposure of normal tissues to the drug (Gupta et al. 2010; Mohanraj and Chen 2006; van Vlerken and Amiji 2006).

The decreased exposure of nonspecific sites or healthy tissues to the drug in NP reduces putative side effects and toxicity (Gupta et al. 2010; Mohanraj and Chen 2006; van Vlerken and Amiji 2006). The enhancement of drug accumulation near the tumor sites is mainly due to the deregulated and leaky nature of tumor vasculature, along with the poor lymphatic drainage. This enhanced permeability and retention effect (EPR) results in passive drug targeting to the tumors and this constitutes a major advantage for NP encapsulated drugs over free drugs. The ideal NP should be biocompatible, selective to tumors and rapidly and efficiently taken up and retained within the cancer cells for sufficient amount of time until it releases its cytotoxic drug cargo and exerts its therapeutic function (Kievit and Zhang 2011; Shapira et al. 2011). Endocytosis is now recognized as the main route for NP entry into cells (Iversen et al. 2011; Oh and Park 2014).

Several TQ-NP formulations have been described in the literature (Bhattacharya et al. 2015; Nair et al. 2010; Rajput et al. 2015; Ravindran et al. 2010; Schneider-Stock et al. 2014). The studies mainly investigated the enhanced anti-inflammatory and anticancer activities of TQ-NP as compared to the free drug. The efficacy of NP formulations is determined by their cell processing mechanism. Several factors influence NP efficacy, including the time and concentration dynamics of NP uptake, the routes of entry, and the trafficking and intracellular distribution. Three studies have addressed TQ-NP-cellular interactions and cell trafficking mechanisms. Guler et al. imaged the uptake of FITC-labeled NP containing *N. sativa* and *Calendula officinalis* extracts by fluorescence microscopy (Guler et al. 2014). siRNA and TQ encapsulated multicellular gold niosome uptake was shown to be time dependent with maximum uptake observed at 180 min, after the particles escaped the lysosomes (Rajput et al. 2015). Bhattacharya et al. demonstrated that PEGylated TQ-NP uptake increased with concentration and was mediated by clathrin-dependent endocytosis (Bhattacharya et al. 2015).

In view of the gap in knowledge regarding TQ-NP interaction with the cells, this project aimed to design TQ-NP and investigate the uptake mechanism and dynamics as well as the TQ-NP fate after cellular trafficking. To this end, TQ was formulated in poly(styrene-*b*-ethylene oxide) (PS-PEO) NP using Flash nanoprecipitation (FNP) (Saad and Prud'homme 2016). PS-PEO is a biocompatible nontoxic amphiphilic diblock copolymer (Ahmad et al. 2010; Cambon et al. 2013; Han et al. 2007). The cytotoxicity and anticancer potential was assessed in normal MCF-10-A breast cells, nonaggressive MCF-7, and highly aggressive MDA-MB-231 human breast cancer cell lines. The classical routes of entry of TQ-NP into cells and the intracellular distribution of the particles after

uptake were investigated in the presence of specific inhibitors and markers of endocytosis.

Experimental

Materials

RPMI 1640, and Dulbecco's Modified Eagle Medium (DMEM) and DMEM-F12 cell culture media were purchased from Lonza (Verviers, Belgium). Thymoquinone, trypsin–EDTA, Dulbecco's phosphate-buffered saline (PBS), horse serum, fetal bovine serum (FBS), penicillin–streptomycin (P/S), epidermal growth factor, hydrocortisone, insulin, cholera toxin, DMSO, MTT (3-(4,5-Dimethylthiazol-2-yl)-2,5-diphenyltetrazolium bromide), trypan blue, methanol, acetonitrile (ACN) HPLC-grade, nile red (NR), chlorpromazine hydrochloride, nystatin, genistein, and amiloride were purchased from Sigma Aldrich (St Louis, Missouri, USA). Hoechst stain was purchased from Molecular Probes, Invitrogen (Eugene, Oregon, USA). Tetrahydrofuran (THF) (99.8 %) was obtained from Acros organics (New Jersey, USA). PS-PEO diblock copolymers were purchased from Polymer Source Inc. (Dorval, Montreal, Canada). Caveolin 1N-20 rabbit polyclonal, transferrin H-65 rabbit polyclonal, EEA-1 E-8 mouse monoclonal IgG, and lamp-1 H4A3 mouse monoclonal IgG antibodies were purchased from Santa Cruz Biotechnology (Paso Robles, California, USA). Alexa Fluor 647 antirabbit IgG and Alexa Fluor 647 antimouse IgG antibodies were purchased from Abcam (Cambridge, UK).

Cell culture

MCF-10 normal breast cells were grown in DMEM/F-12 cell culture media supplemented with 1 % penicillin/streptomycin (P/S with penicillin at 10,000 units and streptomycin at 10 mg/ml), 5 % horse serum, 20 ng/ml epidermal growth factor, 0.5 mg/ml hydrocortisone, 100 ng/ml cholera toxin, and 10 μg/ml insulin. MDA-MB-231 breast cancer cells were grown in RPMI 1640 cell culture media supplemented with 10 % heat-inactivated FBS and 1 % P/S. MCF-7 breast cancer cells were grown in DMEM cell culture media supplemented with 10 % heat-inactivated FBS and 1 % P/S. All cells were maintained in a humidified

atmosphere of 5 % CO_2 at 37 °C. TQ was dissolved in methanol and then diluted in media as needed such that the final methanol concentration did not exceed 0.1 %.

Preparation of TQ-NP

TQ-NP were prepared by FNP using a multiple inlet vortex mixer (MIVM) and controlled flow rates (D'Addio et al. 2012). The formulations were composed of TQ and amphiphilic diblock copolymers of PS-PEO dissolved in 100 % THF. TQ weight ratio to the polymer was 1:1 at a concentration of 50 mg/ml in the THF stream. The solution was rapidly mixed with water using a four-port MIVM with flow rates set at 12/108 ml/min (solvent/water). The flow rates were controlled using Harvard apparatus PHD2000 syringe pumps. Fluorescent TQ-NP were prepared as above, with addition of NR at a concentration of 0.1 mg/ml.

Characterization of TQ-NP

The hydrodynamic particle size was determined by dynamic light scattering (DLS) at 25 °C using 90Plus/BI-MAS (BrookHaven Instruments Corporation (BIC), Holtsville, NY) and analyzed using the BIC particle sizing software in automatic mode. TQ-NP were dispersed in water (1:10) prior to recording the intensity of light scattered at 90° angle to an incident beam. The measured sizes represent the intensity-weighted average value of 3 runs.

To examine the morphology of the TQ-NP, 10 μl of each formulation was deposited on the surface of clean silicon wafers. The silicon plates were air dried in a dark place at room temperature for 24 h before viewing in InBeam mode under the scanning electron microscope (SEM) [from TESCAN, VEGA 3 LMU with OXFORD EDX detector (INCA XMAW20)].

The entrapment efficiency (% EE) and the loading capacity (% LC) of TQ-NP were determined as follows: Amicon Ultra 30 K Ultracel centrifugal filters purchased from Merck Millipore (Tullagreen, Carrigtwohill, IRL) were used according to the manufacturer's guidelines to separate free TQ from TQ in NP. The amount of TQ in the formulation (Total drug) and the amount of TQ in the NP were quantified by high-performance liquid chromatography (HPLC). Equation (1) was used to determine the % EE:

$$\%EE = (\text{Amount of TQ in NP}/\text{Total drug}) \times 100. \tag{1}$$

To measure the loading capacity, 1 ml of formulation was centrifuged using the Amicon Ultra 30 K Ultracel centrifugal filters. The recovered NP were dried by heating prior to weighing. The weight of the NP was integrated in Eq. (2) to calculate the % LC:

$$\%LC = (\text{Amount of TQ in NP}/\text{Nanoparticle weight}) \times 100. \tag{2}$$

Quantification of TQ

TQ-NP formulations were dissolved in THF (100 %) to ensure complete TQ solubilization prior to quantification by HPLC. Chromatographic analysis was conducted on an Agilent Technologies (Walborn, Germany) 1100 series instrument, composed of a vacuum degasser, an autosampler, a quaternary pump, and a diode array detector. Chromatographic separation was performed on a BDS HYPERSIL C_{18} column (250 × 4.6 mm I.D) with 5-μm packing material purchased from Thermo Fisher Scientific (Germany). The samples were eluted at 25 °C using an isocratic mobile phase of water (>18 MΩ resistivity): ACN (45: 55 % v/v) at a flow rate of 1 ml/min. The injection volume was 20 μl and analysis was performed at 254 nm wavelength with a total run time of 15 min. At these conditions, TQ elution time was 7.42 min. Data acquisition, data handling, and instrument control were performed using the Chemstation software package (Agilent). The TQ concentration in the formulation was calculated from a TQ calibration curve obtained by plotting the peak area of the analytical standards 1.5, 3, 30, 75, 150, 300, and 500 μg/ml of TQ prepared in HPLC-grade acetonitrile against their respective TQ concentrations. TQ is light and heat sensitive, and therefore, all samples were protected from light by aluminum foil and prepared on ice in order to avoid TQ degradation. Also, all samples were filtered through 0.2-μm syringe filter prior to HPLC analysis.

Viability assay

Viable cells have the ability to reduce the MTT (3-(4,5-Dimethylthiazol-2-yl)-2,5-diphenyltetrazolium bromide) dye, a yellow tetrazole, into a purple insoluble formazan product the absorbance of which is recorded at 595 nm. MTT assay was used to determine the inhibitory effect of TQ, TQ-NP, and blank NP on the viability of MCF-7 and MDA-MB-231 breast cancer cells and nontumorigenic MCF-10-A breast cell line. Cells were seeded in 96-well plates at a density of 10,000 cells well as described previously (Woo et al. 2011). All treatments were performed at 50 % confluency. At 24 h after treatment, the medium was removed and the cells were incubated overnight with an MTT solution (1 mg/ml prepared in PBS). The solution containing the MTT dye was removed the next day and replaced by isopropanol to dissolve the formazan crystal prior to measuring the colorimetric absorbance of the different wells at 595 nm using a microplate reader (Sutton et al. 2012). Cellular viability was expressed as percentage of cell viability of treated cells relative to untreated controls.

Cellular uptake

Uptake of fluorescent TQ-NP was determined qualitatively by confocal microscopy and quantitatively by flow cytometry. For confocal microscopy analysis, 10^5 cells/ml were plated on cover slips in 6-well plates, in 2 ml of respective growth medium. After treatment with NR-TQ-NP at the indicated time points and concentrations, the cells were rinsed twice with PBS, and fixed at room temperature for 20 min in 4 % formaldehyde solution. Hoechst (0.5 μg/ml) was used to stain the nuclei before mounting on glass slide using FluorSave mounting reagent (Calbiochem). Imaging and visualization as well as Z-stack tomographic sections along the Z-axis were obtained using the Zen software of the Zeiss 710 Confocal microscope (Zeiss, Germany) and a ×63 oil objective.

For fluorometry, 10^5 cells/ml were plated in 6-well plates in 2 ml of respective growth medium. At different time points after treatment with the corresponding amount of NR-TQ-NP, the cells were rinsed twice with PBS, trypsinized, harvested, and then resuspended in 700 μl PBS. The mean fluorescence intensity of cellular uptake was measured using a fluorescence-activated cell sorting (FACS) flow cytometer (Becton–Dickinson BD, FACS Aria Cell Sorter, USA) operated at an excitation of 488 nm and an emission wavelength of 570 nm.

For the competition assay, 10^5 cells/ml were seeded in six well plates in 2 ml of respective growth medium. After overnight incubation, the cells were treated for 5 min with 50 μg/ml NR-TQ-NP, 50 μg/ml NR-TQ-NP + 50 μg/ml TQ, or 50 μg/ml NR-TQ-NP + 50 μg/ml TQ-NP prepared in PBS. After removal of treatment, the cells were rinsed with PBS, trypsinized, harvested, and resupended in 700 μl PBS for fluorometry analysis.

Uptake mechanism

Cells were seeded in 6-well plates at a density of 10^5 cells/ml in 2 ml of respective growth medium and allowed to grow. On the day of treatment, the medium was removed and the cells were separately incubated with PBS containing either chlorpromazine hydrochloride (10 mg/ml), genistein (50 mg/ml), nystatin (50 mg/ml), or amiloride (20 mg/ml) for 1 h before treatment with the fluorescent TQ-NP for 30 min. Finally, cells were washed twice with PBS, trypsinized, harvested, and resuspended in 700 μl of PBS. Cells that were not treated with the inhibitors were used as control. The cellular uptake efficiency was determined using a FACS flow cytometer operated at an excitation wavelength of 488 nm and an emission wavelength of 570 nm.

Subcellular localization

Cells were plated on cover slips in six well plates at a density of 10^5 cells/ml. After overnight incubation in 2 ml of respective growth medium, the medium was removed and the cells were treated for 30 min with 25 μg/ml NR-loaded TQ-NP prepared in PBS. After treatment, the cells were washed twice with PBS and fixed at room temperature for 20 min in 4 % formaldehyde. The formaldehyde was then removed and the cells were washed three times in PBS before permeabilization in 0.2 % Triton solution for 10 min. After two successive 5-min washes in PBS, the cells were blocked in 2 % BSA for 2 h. Caveolin, transferrin, lamp-1, and EEA-1 antibodies were subsequently diluted (1:100) in 1 % BSA and incubated separately with the cells overnight at 4 °C. The next day, the primary antibodies were removed and the cells were washed twice before incubation for 1 h with mouse or rabbit secondary antibodies diluted (1:200) in 0.2 % BSA. Finally, the secondary antibody was removed

and the cells were washed twice in PBS before staining the nuclei with Hoechst (0.5 μg/ml). Coverslips were mounted on glass slides using FluorSave mounting reagent (Calbiochem). Imaging and visualization were done using a Zeiss 710 Confocal microscope (Zeiss, Germany) with a ×63 oil objective.

Statistical analysis

All experiments were performed at least three times. Data are presented as mean ± standard error (SE). Viability was analyzed by one-way Analysis of variance (ANOVA) for comparison of several means with associated post hoc Tukey, and Student–Newman–Keuls (SNK) tests (SPSS Version 16.0). Stability and uptake were analyzed by ANOVA with associated post hoc Dunnett's test to compare to a control. Statistical significance was set at p value ≤ 0.05.

Results

Physicochemical properties of TQ-NP

FNP generates stable TQ-NP with high % EE and % LC

TQ-NP were formulated using the $PS_{1600}PEO_{1800}$ amphiphilic diblock polymer. The numbers in subscript denote the block molecular weight (g/mole). The concentration of both TQ and the polymer used for the preparation of the NP was 50 mg/ml (ratio 1:1). SEM images revealed that TQ-NP have a spherical shape and a smooth surface morphology (Fig. 1a). The hydrodynamic particle size of TQ-NP is presented in Table 1. Measurement of the hydrodynamic diameter by DLS showed that the formulation possessed an average diameter size of 100 nm (Table 1). The physicochemical properties which assess the amount of drug encapsulated in NP per amount of total drug (% EE) and the amount of drug encapsulated per NP weight (% LC) were also investigated. TQ-NP had drug % EE around 80 and % LC around 50 %, respectively (Table 1).

The stability of TQ-NP formulation was investigated by monitoring the average diameter sizes over time. Up to 4 weeks, no significant change in the hydrodynamic particle size was noted (Fig. 1b).
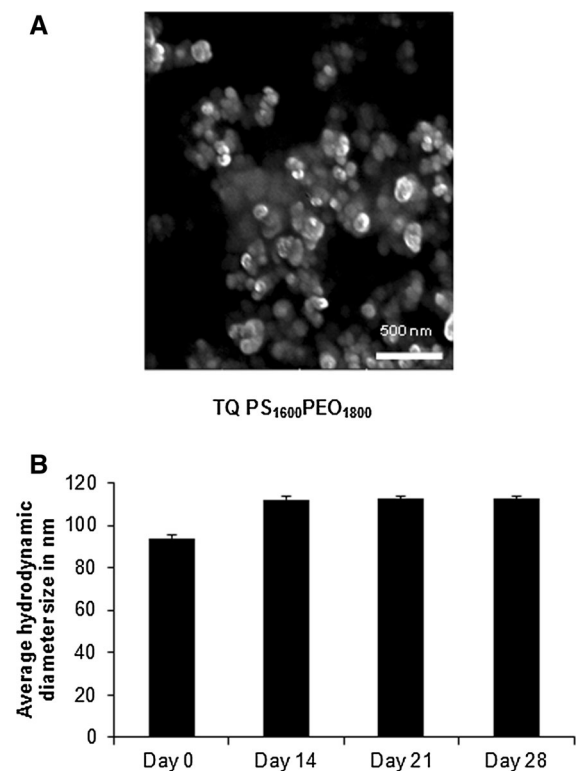
A

TQ PS$_{1600}$PEO$_{1800}$

B

Fig. 1 Preparation of TQ-NP. **a** SEM images showing the morphology of TQ-NP. *Bar* 500 nm. **b** Stability over time of TQ-NP. The data represent the mean of two independent experiments $\pm$ SE ($n = 2$)

Anticancer potential of TQ-NP

TQ-NP are equally or more active than TQ in breast cancer cells and nontoxic to nontumorigenic breast cells

To investigate the anticancer potential of TQ-NP, cells were treated for 24 h with free TQ, TQ-NP, or blank NP at concentrations ranging between 10 and 100 μM of TQ. There was a dose-dependent response to treatment with TQ or TQ-NP in both MCF-7 and MDA-MB-231 breast cancer cells (Fig. 2a, b). With IC$_{50}$ of 30 μM and >100 μM, respectively, the

aggressive MDA-MB-231 breast cancer cell line was more sensitive to treatment with TQ in comparison to MCF-7. This was also the case in response to treatment with TQ-NP. Moreover, in MCF-7, there was clear enhancement of the anticancer activity of TQ-NP over free TQ at 50, 75, and 100 μM starting 24 h with IC$_{50}$ of 70 μM (Fig. 2a). In MDA-MB-231, TQ-NP were as active as free TQ (Fig. 2b). Blank NP did not exhibit any toxicity to both cell lines as shown in Fig. 2a, b. In addition, when tested against normal MCF-10-A breast cell line, TQ and TQ-NP did not affect the viability of these cells up to 25 μM (Fig. 2c). At 50 μM, 24 h after treatment, TQ and TQ-NP slightly decreased cell viability with no significant difference between the viability of cells in response to treatment with free or encapsulated drug. As previously observed with the MCF-7 and MDA-MB-231 breast cancer cells, treatment of MCF-10-A normal cells with blank NP did not cause affect cell viability (Fig. 2c).

Mechanism of cellular uptake of TQ-NP

NR-loaded TQ-NP are internalized by the cells in a time and concentration-dependent manner

To study the cellular uptake of TQ-NP in vitro, NR fluorescent dye was incorporated into the NP formulation (0.1 mg/ml). Commonly used fluorescent dyes are typically hydrophilic, making them incompatible for use with FNP, which relies on imposing high supersaturation levels using water as an antisolvent for precipitating hydrophobic solutes. Nile red is a hydrophobic dye previously used for the labeling and imaging of NP prepared by FNP(Akbulut et al. 2009). As such, TQ-NP containing NR were formulated by FNP. The TQ:NR weight ratio used was (500:1). The fluorescent dye had no significant effect on the size, stability, or % EE and % LC of the TQ-NP formulation (Table 1). Subsequently, tomographic scans of both MCF-7 and MDA-MB-231 cells after incubation with 10 μg/ml of NR-loaded TQ-NP for

Table 1 Characterization of the average hydrodynamic diameter size, the entrapment efficiency, and the loading capacity of TQ-NP

NP	Size (nm)	EE (%)	LC (%)
TQ PS$_{1600}$ PEO$_{1800}$	94.1 $\pm$ 1.7	79.2 $\pm$ 0.2	50.5 $\pm$ 4.6
TQ PS$_{1600}$ PEO$_{1800}$ + NR	115.5 $\pm$ 0.1	79.9 $\pm$ 0.1	49.8 $\pm$ 0.3

The data represent the mean of two independent experiments $\pm$ SE ($n = 2$)
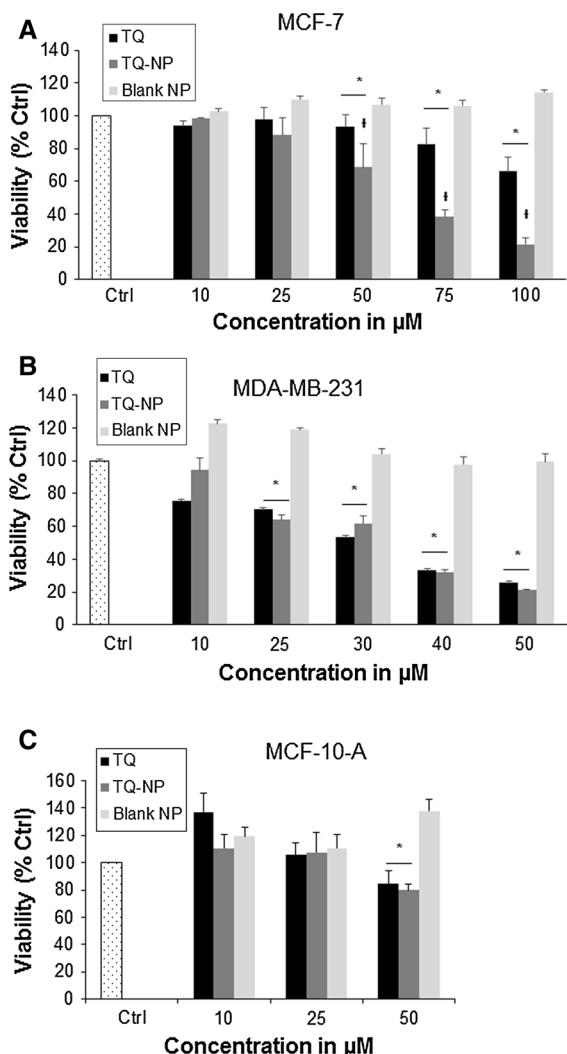
Fig. 2 TQ-NP anticancer potential in vitro. **a** The viability of MCF-7 and MDA-MB-231 breast cancer cells was determined in the presence of TQ and TQ-NP. **b** The viability of MCF-7 and MDA-MB-231 breast cancer cells in response to treatment with blank NP. **c** The viability of nontumorigenic MCF-10 epithelial breast cells in response to treatment with TQ, TQ-NP, or blank NP. All cells were seeded at 100,000 cells/ml in 96-well plates and treated 24 h later with 10–100 μM TQ, TQ-NP, or blank NP. MTT viability assay was performed at 24 h post treatment and the values were normalized to the control. Each condition was done in triplicate and the experiment was repeated twice. The *error bars* represent the standard error. *Asterisk* indicates $p < 0.05$ with respect to the control. † Indicates $p < 0.05$ with respect to TQ

30 min were performed to locate the NP in the cells (Fig. 3a). The different planes on the *z*-axis (Fig. 3a lower panels) as well as the three-dimensional reconstruction (Fig. 3a upper panel) demonstrate that the

NP are internalized by MCF-7 and MDA-MB-231 breast cancer cells and distributed in the cytoplasm and the nucleus. The distribution of a drug inside the cell can be very predictive of its activity, and hence, TQ-NP anticancer activity can be linked to activation of elements in both the cytoplasm and the nucleus.

Determining the maximum concentration of NP taken up by cells is also critical for the design of a treatment regimen for in vivo administration. To this aim, cells were treated for 30 min with either 10 or 25 μg/ml of NR-loaded TQ-NP. As shown in Fig. 3b and Supplementary Fig. 1a, the mean fluorescence intensity (MFI) was increased when the cells were incubated with higher particle concentration. The increase in uptake between the MFI was around twofolds in both cell lines which is proportional to the concentration difference. The MFI after treatment of cells with 50 μg/ml of NR-loaded TQ-NP did not significantly increase as compared with cells treated with 25 μg/ml of NR-loaded TQ-NP (data not shown). A similar result was obtained after quantification of the uptake by confocal microscopy (Supplementary Fig. 1b). These images support the quantitative measurements of the cellular uptake, and reveal a strong fluorescence in the cell cytoplasm and in the nucleus as observed previously through confocal imaging (Fig. 3a).

In addition, nanoparticles for chemotherapy need to be taken up by cells with a sufficiently high rate and extent. To assess the dynamics of this uptake, MCF-7 and MDA-MB-231 cells were incubated with 10 μg/ml of NR-loaded TQ-NP for increasing amounts of time, starting from 5 to 60 min. At the indicated time points, the MFI of the cells was measured by flow cytometry. The data of the overlay in Fig. 3c and the corresponding representative bar graph in Supplementary Fig. 1c indicate that there is a clear increase in the uptake between 5, 15, and 30 min as compared to the nontreated cells in both cell lines. Uptake did not increase between the 30 min and 60 min time points, indicating saturation is reached at 30 min. Hence, these findings indicate that the TQ-NP enter the cells in a time-dependent manner until 30 min of incubation of NP with the cells.

TQ and TQ-NP take different routes for entry into the cells

To determine the amount of cells which incorporate TQ-NP following incubation of the cells with the different treatment conditions, the % positive cell

Fig. 3 Cell uptake of TQ-NP. **a** MCF-7 and MDA-MB-231 breast cancer cells were incubated with 10 μg/ml of NR-loaded TQ-NP in growth medium for 30 min before being prepared for confocal imaging. Images were obtained using a Zeiss 710 confocal microscope and a ×63 oil objective. Four slices taken at different positions on the z-axis are represented in the small panels to illustrate the position of the NP in the cells near the cell surface and or in proximity to the nucleus. Upper panel represents the cells 3D spatial reconstruction created by taking 21 slices on the z-axis, each slice having a thickness of 0.6 um. **b** The effect of particle concentration on the cellular uptake of NR-loaded TQ-NP as expressed by the mean fluorescence intensity of MCF-7 and MDA-MB-231 cells treated with 10 or 25 μg/ml NR-loaded TQ-NP. NR-loaded TQ-NP were prepared in PBS and the treatment was done for 30 min at 37 °C. **c** The effect of particle incubation time on the cellular uptake of NR-loaded TQ-NP as expressed by the mean fluorescence intensity of MCF-7 (*left panel*) and MDA-MB-231 (*right panel*) cells treated with 10 μg/ml of NR-loaded TQ-NP for 0, 5, 15, 30, and 60 min
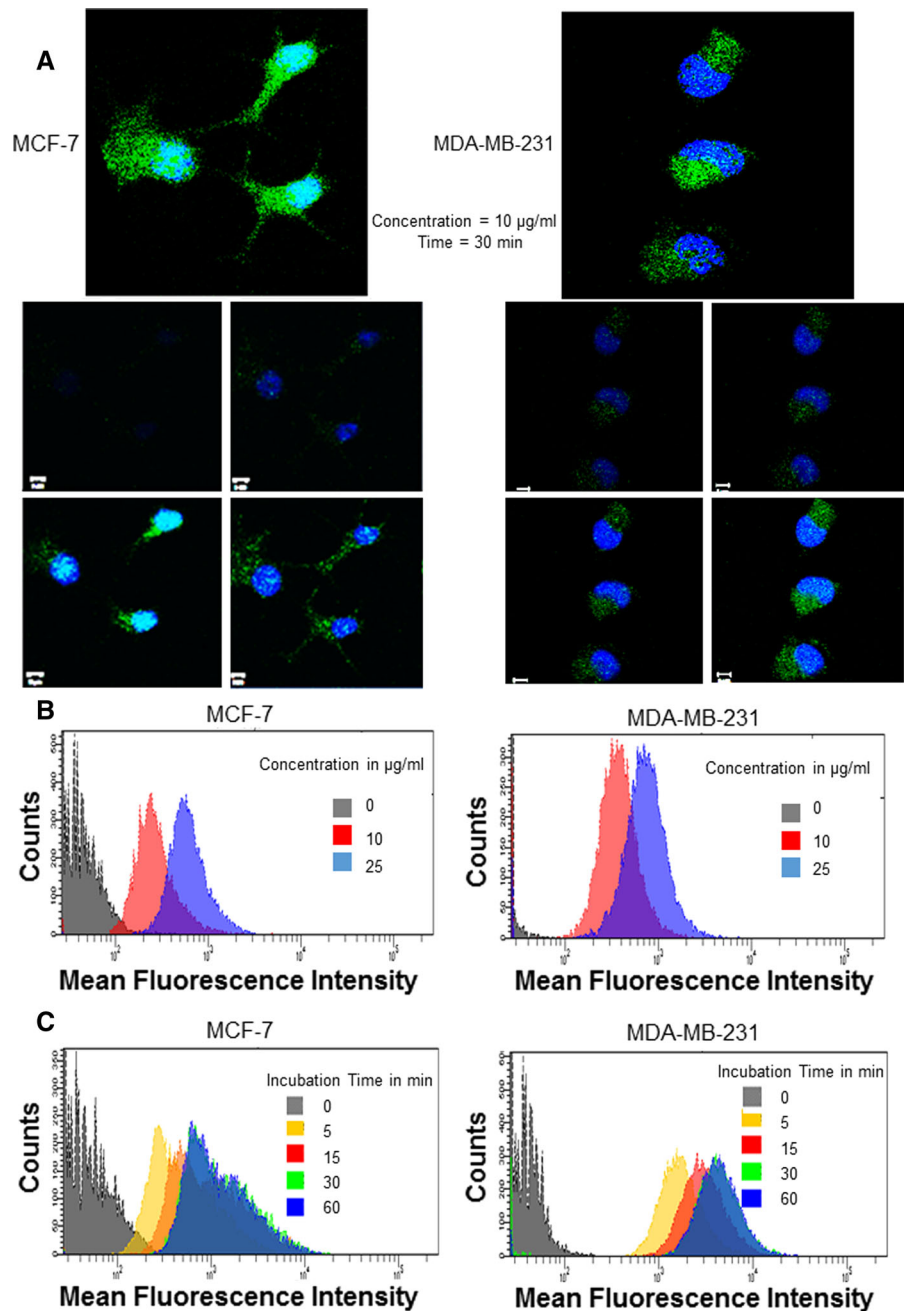
population, in comparison to the untreated control, was investigated (Fig. 4a). In both cell lines, the % positive cells, i.e., the population of cells which had incubated TQ-NP after treatment for 5 min, were very high, whereby around 80 % of MCF-7 cells and approximately 95 % of MDA-MB-231 cells were positive. There was no significant difference in the %

positive cells between 5 and 30 min which reflects the fast uptake of NP by the cells which in majority seem to take up TQ-NP as early as 5 min. To test whether the fast uptake of TQ-NP correlates with the anti-cancer potential of the NP, MDA-MB-231 breast cancer cells were treated with 25 μM TQ or TQ-NP for 30 min. The treatment was then removed and the

cells were incubated with cell culture media after which cell viability was assessed at 24 h post treatment (Fig. 4b). Both TQ and TQ-NP decreased cell viability of MDA-MB-231 breast cancer cells after treatment for 30 min and removal of treatment with TQ-NP causing more inhibition of cell vibility. Specifically, treatment of MDA-MB-231 breast cancer cells for 30 min with TQ-NP results in 40 % cell death while treatment with TQ and removal of treatment only causes around 20 % cell death in MDA-MB-231 breast cancer cells. To demonstrate that the difference in dynamics of uptake of TQ and TQ-NP stems from a difference in the mechanism of uptake of free or encapsulated TQ, a competition assay was performed to test whether TQ and TQ-NP have the same mechanism of uptake inside the cells. To this aim, MCF-7 and MDA-MB-231 breast cancer cells were treated for 5 min with 50 µg/ml NR-loaded TQ-NP alone or in combination with either 50 µg/ml of TQ or 50 µg/ml of TQ-NP. The MFI was measured by fluorometry and the uptake profiles of the different treatment conditions were overlayed (Fig. 4c). NP uptake by MCF-7 and MDA-MB-231 cells is reflected by the shift of the mean fluorescent peak to the right as compared to the untreated control. When cells are treated with NR-loaded TQ-NP and competed with TQ, the MFI peak remains similar to that obtained with cells treated with NR-loaded TQ-NP alone. However, a clear MFI shift to the left is observed for cells treated with fluorescent and nonfluorescent TQ-NP. Quantitatively, the competition accounts for 40 % inhibition of uptake of fluorescent NP in both cell lines (Fig. 4d).

Caveolin and clathrin-dependent endocytosis play a role in TQ-NP uptake

Given that TQ can freely diffuse into the cells, endocytosis, the major route of uptake of NP, was investigated to determine its implication in the uptake of TQ-NP. To this aim, different endocytosis inhibitors were used. Cells were pretreated with nystatin, genistein, chlorpromazine hydrochloride, and amiloride, prior to treatment with NR-loaded TQ-NP. Nystatin depletes cholesterol and inhibits the formation of sag vesicles (Iversen et al. 2011). It is also a caveolae-mediated endocytosis inhibitor (Liu et al. 2014). Genistein inhibits several tyrosine kinases and enables the disruption of the caveolin-mediated
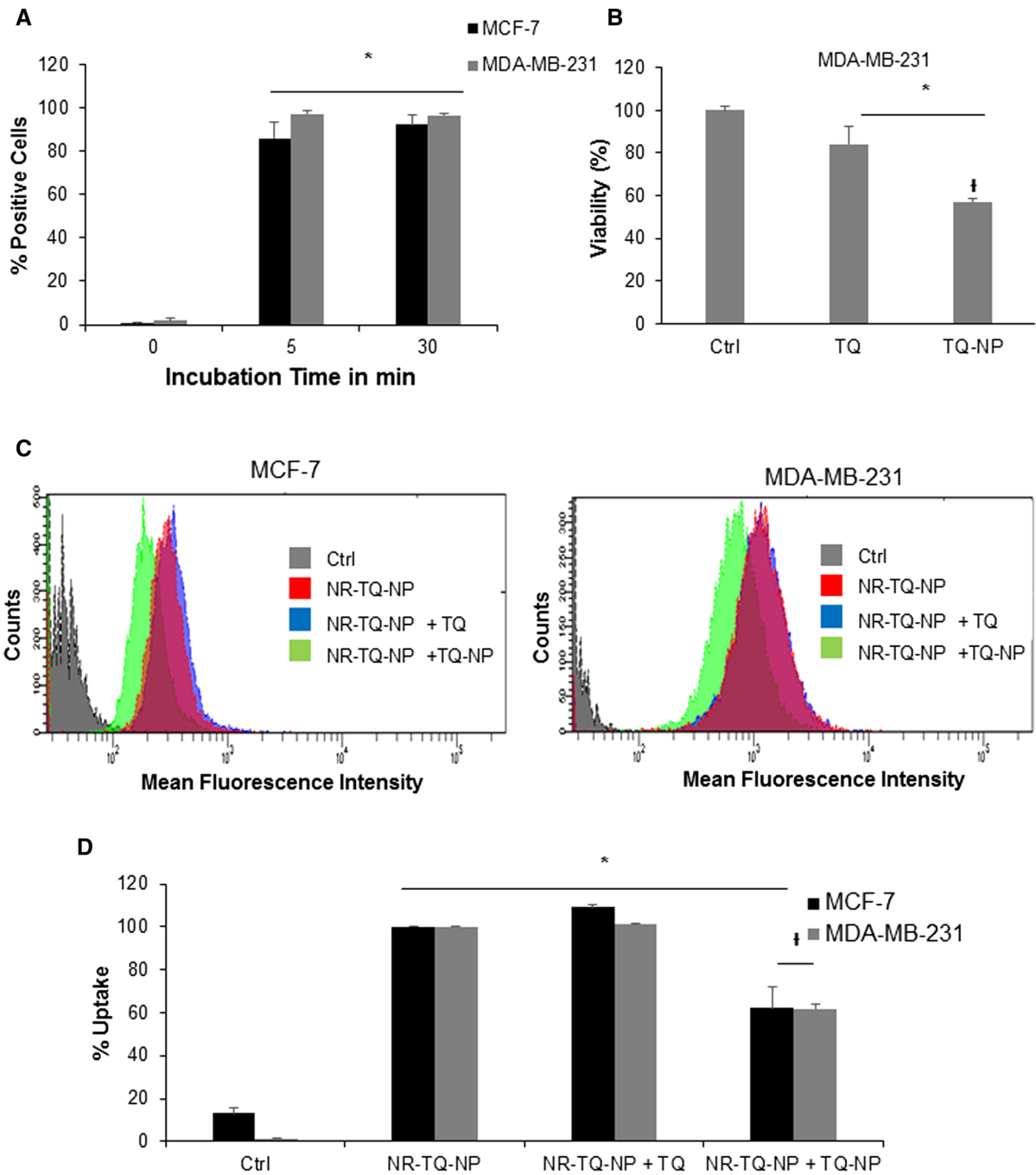
endocytosis, or lipid rafts route (Iversen et al. 2011; Liu et al. 2014). Chlorpromazine hydrochloride is an inhibitor of Rho GTPases which prevents the formation of clathrin-coated sag vesicles, and thus disturbs the clathrin-mediated endocytosis (Iversen et al. 2011; Liu et al. 2014; Zeng et al. 2014). Finally, amiloride is a blocker of micropinocytosis which functions by lowering the pH close to the membrane and preventing Rac1 and Cdc42 signaling (Iversen et al. 2011; Liu et al. 2014; Zeng et al. 2014). Treatment with genistein reduced the uptake of NP in MCF-7 cells by 20 % as shown in Fig. 5a. The same trend was observed in MDA-MB-231 cells where this decrease was slightly more pronounced (around 30 %) and where an inhibition of the uptake was also observed in response to treatment with chlorpromazine (Fig. 5a).

NP can be processed by endosomes and lysosomes

To rule out any nonspecificity effect of the inhibitors of endocytosis, the internalization of TQ-NP was investigated. The cellular trafficking and biodistribution of TQ-NP after entry into cells was also determined using the following markers: caveolin to label the caveolae, transferrin to detect the clathrin-coated pits as well as early and recycling endosomes, early endosome antigen 1 (EEA-1) to identify early endosomes, and lysosomal-associated membrane protein 1 (lamp-1) for lysosomes tracking. Figure 5b and Supplementary Fig. 2 show that the NP colocalize with caveolin, transferrin, as well as with EEA-1 and lamp-1 in both cell lines. These findings further provide evidence for the role of caveolin- and clathrin-mediated endocytosis in the uptake of TQ-NP as well as highlight the involvement of the endosomes and lysosomes in the trafficking and cargo delivery.

Discussion

This is the first comprehensive study of the cellular uptake mechanisms, the trafficking, and the spatial distribution of fluorescent TQ-NP. In this study, polymeric TQ-NP were prepared using PS-PEO diblock copolymer via FNP. This formulation was nontoxic to nontumorigenic MCF-10-A breast cell line up to 25 µM and showed equal or enhanced activity against MDA-MB-231 and MCF-7 breast cancer cell lines, respectively, in comparison to free TQ. Uptake

A

% Positive Cells vs Incubation Time in min (MCF-7, MDA-MB-231)

B

MDA-MB-231 — Viability (%) for Ctrl, TQ, TQ-NP

C

MCF-7 and MDA-MB-231 — Counts vs Mean Fluorescence Intensity (Ctrl, NR-TQ-NP, NR-TQ-NP + TQ, NR-TQ-NP +TQ-NP)

D

% Uptake for Ctrl, NR-TQ-NP, NR-TQ-NP + TQ, NR-TQ-NP + TQ-NP (MCF-7, MDA-MB-231)

studies suggest that inhibiting caveolin-dependent endocytosis reduces the uptake of TQ-NP by 20–30 % in MCF-7 and MDA-MB-231 cells and that caveolin-dependent endocytosis as well as clathrin-dependent endocytosis are implicated in the uptake of TQ-NP in MDA-MB-231 breast cancer cells. Following internalization, TQ-NP can be found colocalizing with both endosomes (EEA-1) and lysosomes (Lamp-1).

The polymeric TQ-NP formulation described in this study holds great potential for in vivo application

◀ **Fig. 4** Uptake and anticancer potential of TQ vs TQ-NP. **a** MCF-7 and MDA-MB-231 breast cancer cells were incubated with 10 µg/ml of NR-loaded TQ-NP for 5 and 30 min. The NP were prepared for flow cytometry as mentioned above. The % positive cell population of NR-loaded TQ-NP treated cells was determined in reference to the control untreated cells. The data represent the mean of two independent experiments ± SE ($n = 3$). Asterisk indicates $p < 0.05$ with respect to the untreated control (0), **b** MDA-MB-231 breast cancer cells were seeded at 100,000 cells/ml in 96 well plates and treated 24 h later with 25 µM of TQ, TQ-NP or blank NP. After 30 min incubation with the cells, the treatment was removed and replaced with cell culture media. Cell viability was assessed 24 h post treatment by MTT assay. The values were normalized to the control. Each condition was done in triplicate and the experiment was repeated three times. The *error bars* represent the standard error. Asterisk indicates $p < 0.05$ with respect to the control. † Indicates $p < 0.05$ with respect to TQ. **C.** MCF-7 and MDA-MB-231 breast cancer cells were incubated for 5 min with 50 µg/ml of NR-loaded TQ-NP, or a mixture of 50 µg/ml of NR-loaded TQ-NP and 50 µg/ml TQ, or a mixture of 50 µg/ml of NR-loaded TQ-NP and 50 µg/ml TQ-NP. The NP were prepared in PBS and the treatment was done at 37 °C. After incubation, the cells were prepared for flow cytometry analysis and the fluorescence intensity was measured at 488 nm excitation and 570 emission. A representative histogram featuring the mean fluorescence intensity of control and treated cells is shown on the left for MCF-7 cells and on the right for MDA-MB-231 cells (**d**). *Bar* graph showing the competition assay of the uptake of NR-loaded TQ-NP expressed as the average of the mean fluorescence intensity of MCF-7 and MDA-MB-231 cells ± SE. The data represent two independent experiments ($n = 3$). Asterisk indicates $p < 0.05$ with respect to the control. † Indicates $p < 0.05$ with respect to NR-TQ-NP

owing to their small size, long-term stability, and ability to be internalized to the cytoplasm and reach the nucleus of cells. Size control, high % EE and % LC are additional advantages conferred by the TQ-NP preparation described in the present work. Flash nanoprecipitation thus enabled the preparation of TQ-NP with average diameters suitable for cancer drug delivery applications as they are large enough to escape elimination by the kidney (>10 nm) and small enough to be sterilized (<200 nm) (Lammers et al. 2012; Nair et al. 2010; Shekunov et al. 2007). In comparison, large TQ-NP were reported in previous studies (Abu-Dahab et al. 2013; Alam et al. 2012; Ravindran et al. 2010; Shah et al. 2011). Moreover, while some previously published TQ-NP papers do not assess the % EE and % LC of the formulations, FNP enabled the formulation of TQ-NP with considerably greater % EE and % LC than other polymeric and chitosan-based TQ-NP (Alam et al. 2012; Ganea et al. 2010; Shah et al. 2010). Finally, the findings show that

the TQ-NP formulations stability is maintained through steric stabilization provided by PS-PEO over 4 weeks which can potentially minimize nonspecific interactions and prevent NP loss and side toxicity (Nair et al. 2010). The ethylene oxide component of the diblock copolymer is also expected to impart 'stealth' capability to the NP.

Previously described TQ-NP have been tested against both MDA-MB-231 and MCF-7 cancer cell lines and have been shown to either have greater activity (Abu-Dahab et al. 2013; Dehghani et al. 2015; Ganea et al. 2010; Ravindran et al. 2010) or equal activity (Bhattacharya et al. 2015) in comparison to free TQ. For instance, a twofold increase in the activity of TQ-NP in MDA-MB-231 at 96 h was reported by Ganea et al. (2010). The lack of enhancement in drug activity of PS-PEO TQ-NP in MDA-MB-231 cells observed in the present work is most likely due to the high sensitivity of these cells to TQ or to the difference in the genetic background of these cells. In the case of MCF-7 cells, Odeh et al. (2012) have shown that liposomal TQ had much lower anticancer activity than free TQ, with an ED_{50} five times higher than that of free TQ (Odeh et al. 2012), while Bhattacharya et al. (2015) reported similar anticancer potential of TQ-NP in comparison to free TQ. Yet, the advantage of the latter formulation was its reduced cytotoxicity to normal PBMC cells (Bhattacharya et al. 2015). Some formulations that increased TQ's anticancer potential in MCF-7 cells had larger average particle sizes. This was the case of beta-cyclodextrin TQ-NP (TQ-CD) which were sixfolds more active than TQ in inhibiting MCF-7 cell viability at 72 h (Abu-Dahab et al. 2013).

Imaging of TQ-NP in breast cancer cells revealed that NR-labeled TQ-NP clearly internalize inside the cells. They were shown to accumulate both in the cytoplasm as well as in the nucleus, and hence, their activity can be linked to activation of elements in both compartments. Given that only small NP can pass the nuclear pore complexes which are around 10–25 nm in diameter (Elsabahy and Wooley 2012), the data suggest that the smaller particles of the NP size distribution have freely diffused to those compartments and/or that a reduction in size of the NP has occurred. Drug diffusion from the NP to the cytoplasm and the nucleus after cellular intake could account for NP size reduction. The distribution of the NP inside the cells can be very predictive of their mechanism of action.
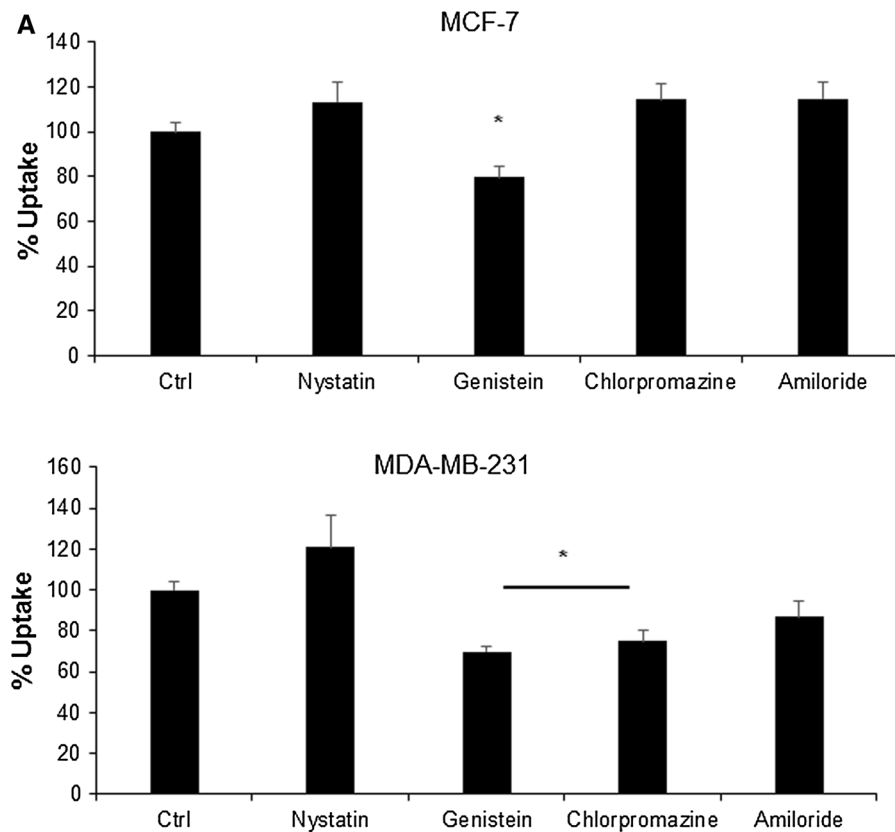
A MCF-7

Fig. 5 TQ-NP uptake by caveolin-mediated endocytosis pathway. **a** Effect of the inhibitors of endocytosis on the internalization of NR-loaded TQ-NP by MCF-7 and MDA-MB-231. Cells were untreated (Ctrl) or pretreated with nystatin (50 mg/ml), genistein (50 mg/ml), chlorpromazine (10 mg/ml), or amiloride (20 mg/ml), for 1 h prior to treatment with NR-loaded TQ-NP (10 μg/ml) for 30 min. After treatment, the mean fluorescence intensity of each condition was measured by flow cytometry. The uptake is expressed as percentage of the mean fluorescence intensity relative to the untreated control ± SE. All experiments were done at least in duplicate ($n = 3$) and Dunnett's test was used for statistical analysis, *$p < 0.05$. **b** The intracellular distribution of NR-loaded TQ-NP. MDA-MB-231 breast cancer cells were incubated with 25 μg/ml of NR-loaded TQ-NP in growth medium for 30 min before preparation for incubation with the primary antibodies of the different endocytic markers (dilution 1:100). Caveolin, transferrin, EEA-1, and Lamp-1 are visualized in *red*, the NP in *green*, and the nuclei stained with Hoechst are shown in *blue*. The images were obtained using a Zeiss 710 confocal microscope and a ×63 oil objective. *Bar* 5 μm. (Color figure online)

Furthermore, NR-labeled TQ-NP uptake in breast cancer cells was shown to be time and concentration dependent. The uptake time represents the time required for the particles to come into contact with the cell membranes, the time for packaging the NP, and their entry into the cells (Kievit and Zhang 2011). In both cases, the uptake reached a maximum beyond which a plateau effect was observed. Saturation of the cells with NP or an equilibrium between NP uptake and their excretion by the cells could account for the plateau effect. The trend of increasing uptake with increasing concentration is in line with recently reported results for PEG TQ-NP uptake in the low concentration range (Bhattacharya et al. 2015).

In addition, the fast uptake revealed by the high percentage of positive cells at 5 min was shown to account for the enhanced anticancer potential of TQ-NP as compared with free TQ in MDA-MB-231 breast cancer cells. Indeed, treatment of MDA-MB-231 breast cancer cells with TQ or TQ-NP for 30 min followed by removal of treatment indicated that both TQ and TQ-NP are taken up by the cells at this incubation time. However, treatment with TQ-NP before removal of treatment caused an inhibition of
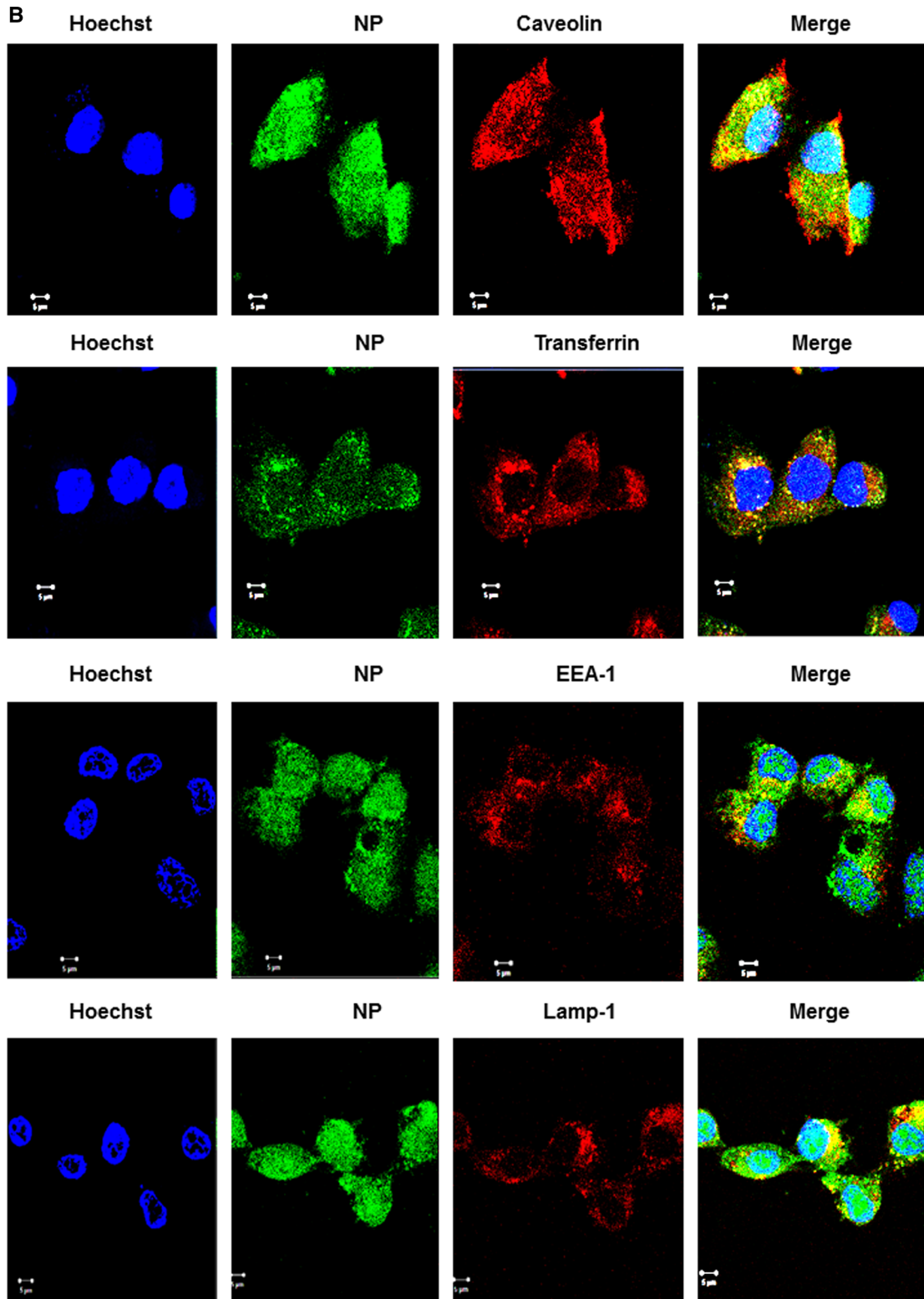
Fig. 5 continued

cell viability similar to that observed with cells treated with TQ-NP for 24 h, while treatment with TQ and removal of treatment only caused around 20 % cell death which is significantly different from the effect of treatment of MDA-MB-231 breast cancer cells with TQ for 24 h. This difference attributed to the fast uptake of TQ-NP as compared with free TQ confirms thus the advantage of TQ encapsulation. Moreover, the inhibition of uptake of labeled TQ-NP by cotreatment with the unlabeled ones provided evidence that TQ-NP and NR-loaded TQ-NP are taken up by the same pathway in MDA-MB-231 and MCF-7 breast cancer cells. The competition assay further showed that TQ and TQ-NP enter the cells using different routes, suggesting the involvement of endocytosis in the uptake of TQ-NP.

Encapsulation of therapeutic agents into NP with a particular affinity for an internalization pathway has the potential to increase the efficiency of membrane targeting given that the route of entry of nanocarriers in the cells has a direct impact on their fate after internalization (Kievit and Zhang 2011; Xu et al. 2013). The use of inhibitors of endocytosis as well as the colocalization studies suggests a role for caveolin-dependent endocytosis in mediating the uptake of TQ-NP in MCF-7 and MDA-MB-231 cells and a clathrin-dependent endocytosis role in mediating the uptake of TQ-NP in MDA-MB-231 cells. Clathrin-mediated endocytosis in MCF-7 cells has been reported recently (Bhattacharya et al. 2015). The results obtained with NR-loaded TQ-NP are consistent with previous results showing that the uptake of polystyrene nanoparticles by HeLa and human umbilical vein endothelial cells is clathrin and or caveolin dependent (Lai et al. 2007). Additionally, a high expression of caveolin in breast cancer cells might account for the involvement of caveolae in the uptake of TQ-NP (Chung et al. 2015).

Interestingly, neurons and leukocytes do not express caveolins or possess caveolae, which ensures, in case of in vivo application of NR-loaded TQ-NP, no toxicity side effects at those specific tissues (Xu et al. 2013). Nanomaterials that enter the cells in a caveolin-dependent manner can be delivered to the ER and subsequently the cytosol, and enter the nucleus via the nuclear pore complex (Xu et al. 2013). Compared with clathrin-dependent endocytosis, the trafficking along this pathway is longer and the nanomaterial are subjected to less degradation resulting in enhanced drug concentration, delivery to target organelles, and

thus overall improvement of therapeutic effect (Kou et al. 2013). However, the inhibitors of endocytosis and the colocalization studies might not be specific enough, and hence the need to investigate the uptake of TQ-NP in cells expressing mutated proteins or the use of siRNA to target the different pathways of endocytosis for a conclusive understanding of TQ-NP mechanism of uptake.

The multifunctional nature of the polymeric TQ-NP prepared in this study opens up the possibility of improved clinical outcomes that may not be achievable with the administration of TQ in its free form. For instance, Abraxane, is an albumin bound paclitaxel formulation that has reached the market for the treatment of breast and pancreatic neoplasma (Ryan and Brayden 2014). Several polymeric drug carriers have also received regulatory approval for breast cancer treatment including formulations of doxorubicin, camptothecin, and other polymeric formulations of paclitaxel (Ryan and Brayden 2014).

In addition to the therapeutic advantage of TQ-NP, the NR-labeled TQ-NP developed in this study allows for imaging of the particles inside the cells. Flash nanoprecipitation can be exploited to produce multifunctional NP affording coformulation of imaging and anticancer agents, which is of great use in nanotheranostics, which integrates diagnostics and therapeutics in one system (Kim et al. 2013). For translation to the clinic, drug carriers that enable imaging are more advantageous than therapeutic NP alone given that physicians can monitor drug concentrations in off-target organs and in the tumor to adjust the type and dosing of drug for each patient and prevent over or under treatment that could result in harmful side effects or incomplete cancer remission (Kievit and Zhang 2011).

The colocalization of TQ-NP with both endosomes (EEA-1) and lysosomes (Lamp-1) indicates that TQ-NP translocate from the endosomes and lysosomes to the cytoplasm after entering the cells by endocytosis. The process related to endosome maturation might therefore account for the accessibility of TQ in NP form to the cytoplasm and the nucleus where they exert their anticancer activity in both compartments (Iversen et al. 2011).

In summary, the multifunctional nature of the polymeric TQ-NP prepared in this study enables the imaging as well as the treatment of different cell lines which cannot be achievable with the administration of

TQ in its free form. Furthermore, the overall advantages of the PS-PEO TQ-NP formulation in terms of size, stability, anticancer potential, and dynamics of cellular uptake as well as their ability to be internalized to the cytoplasm and reach the nucleus of cells make it a potential candidate for cancer treatment, and hence the need for further in vivo evaluation which is currently being undertaken.

References

Abu-Dahab R, Odeh F, Ismail SI, Azzam H, Al Bawab A (2013) Preparation, characterization and antiproliferative activity of thymoquinone-beta-cyclodextrin self assembling nanoparticles. Pharmazie 68:939–944

Ahmad F, Baloch MK, Jamil M, Jeon YJ (2010) Characterization of polystyrene-b-poly(ethylene oxide) diblock copolymer and investigation of its micellization behavior in water. J Appl Polymer Sci. doi:10.1002/app.32165

Akbulut M, Ginart P, Gindy ME, Theriault C, Chin KH, Soboyejo W, Prud'homme RK (2009) Generic method of preparing multifunctional fluorescent nanoparticles using flash nanoprecipitation. Adv Funct Mater 19:718–725. doi:10.1002/adfm.200801583

Alam S, Khan ZI, Mustafa G, Kumar M, Islam F, Bhatnagar A, Ahmad FJ (2012) Development and evaluation of thymoquinone-encapsulated chitosan nanoparticles for nose-to-brain targeting: a pharmacoscintigraphic study. Int J Nanomed 7:5705–5718. doi:10.2147/ijn.s35329

Bhattacharya S et al (2015) PEGylated-thymoquinone-nanoparticle mediated retardation of breast cancer cell migration by deregulation of cytoskeletal actin polymerization through miR-34a. Biomaterials 51:91–107 doi:10.1016/j.biomaterials.2015.01.007

Brannon-Peppas L, Blanchette JO (2004) Nanoparticle and targeted systems for cancer therapy. Adv Drug Deliv Rev 56:1649–1659. doi:10.1016/j.addr.2004.02.014

Cambon A et al (2013) Poly(styrene oxide)-poly(ethylene oxide) block copolymers: from "classical" chemotherapeutic nanocarriers to active cell-response inducers. J Control Release 167:68–75. doi:10.1016/j.jconrel.2013.01.010

Chung YC, Kuo JF, Wei WC, Chang KJ, Chao WT (2015) Caveolin-1 dependent endocytosis enhances the chemosensitivity of HER-2 positive breast cancer cells to Trastuzumab Emtansine (T-DM1). PloS one 10:e0133072. doi:10.1371/journal.pone.0133072

D'Addio SM et al (2012) Effects of block copolymer properties on nanocarrier protection from in vivo clearance. J Controll Release 162:208–217. doi:10.1016/j.jconrel.2012.06.020

Dehghani H, Hashemi M, Entezari M, Mohsenifar A (2015) The comparison of anticancer activity of thymoquinone and nanothymoquinone on human breast adenocarcinoma Iranian. J Pharm Res 14:539–546

Elsabahy M, Wooley KL (2012) Design of polymeric nanoparticles for biomedical delivery applications. Chem Soc Rev 41:2545–2561. doi:10.1039/c2cs15327k

Ganea GM, Fakayode SO, Losso JN, van Nostrum CF, Sabliov CM, Warner IM (2010) Delivery of phytochemical thymoquinone using molecular micelle modified poly(D, L lactide-co-glycolide) (PLGA) nanoparticles. Nanotechnology 21:285104. doi:10.1088/0957-4484/21/28/285104

Guler E et al (2014) Bio-active nanoemulsions enriched with gold nanoparticle, marigold extracts and lipoic acid: in vitro investigations Colloids and surfaces B. Biointerfaces 121:299–306. doi:10.1016/j.colsurfb.2014.05.026

Gupta VK, Karar PK, Ramesh S, Misra SP, Gupta A (2010) Nanoparticle formulation for hydrophilic & hydrophobic drugs. Int J Res Pharm 1:163–169

Han K, Miah MA, Shanmugam S, Yong CS, Choi HG, Kim JA, Yoo BK (2007) Mixed micellar nanoparticle of amphotericin B and poly styrene-block-poly ethylene oxide reduces nephrotoxicity but retains antifungal activity. Arch Pharm Res 30:1344–1349

Iversen T-G, Skotland T, Sandvig K (2011) Endocytosis and intracellular transport of nanoparticles: present knowledge and need for future studies. Nano Today 6:176–185. doi:10.1016/j.nantod.2011.02.003

Kievit FM, Zhang M (2011) Cancer nanotheranostics: improving imaging and therapy by targeted delivery across biological barriers. Adv Mater (Deerfield Beach, Fla) 23:H217–247 doi:10.1002/adma.201102313

Kim TH, Lee S, Chen X (2013) Nanotheranostics for personalized medicine. Expert Rev Mol Diagn 13:257–269. doi:10.1586/erm.13.15

Kou L, Sun J, Zhai Y, He Z (2013) The endocytosis and intracellular fate of nanomedicines: Implication for rational design. Asian J Pharm Sci 8:1–10. doi:10.1016/j.ajps.2013.07.001

Lai SK, Hida K, Man ST, Chen C, Machamer C, Schroer TA, Hanes J (2007) Privileged delivery of polymer nanoparticles to the perinuclear region of live cells via a non-clathrin, non-degradative pathway. Biomaterials 28:2876–2884. doi:10.1016/j.biomaterials.2007.02.021

Lammers T, Kiessling F, Hennink WE, Storm G (2012) Drug targeting to tumors: principles, pitfalls and (pre-) clinical progress. J Control Release 161:175–187 doi:10.1016/j.jconrel.2011.09.063

Liu P, Sun Y, Wang Q, Sun Y, Li H, Duan Y (2014) Intracellular trafficking and cellular uptake mechanism of mPEG-PLGA-PLL and mPEG-PLGA-PLL-Gal nanoparticles for targeted delivery to hepatomas. Biomaterials 35:760–770. doi:10.1016/j.biomaterials.2013.10.020

Lopez-Davila V, Seifalian AM, Loizidou M (2012) Organic nanocarriers for cancer drug delivery. Curr Opin Pharmacol 12:414–419. doi:10.1016/j.coph.2012.02.011

Mohanraj VJ, Chen Y (2006) Nanoparticles—a review. Trop J Pharm Res 5:561–573. doi:10.4314/tjpr.v5i1.14634

Nair HB, Sung B, Yadav VR, Kannappan R, Chaturvedi MM, Aggarwal BB (2010) Delivery of antiinflammatory nutraceuticals by nanoparticles for the prevention and treatment of cancer. Biochem Pharmacol 80:1833–1843. doi:10.1016/j.bcp.2010.07.021

Odeh F, Ismail SI, Abu-Dahab R, Mahmoud IS, Al Bawab A (2012) Thymoquinone in liposomes: a study of loading efficiency and biological activity towards breast cancer. Drug Delivery 19:371–377. doi:10.3109/10717544.2012.727500

Oh N, Park JH (2014) Endocytosis and exocytosis of nanoparticles in mammalian cells. Int J Nanomed 9(Suppl 1):51–63. doi:10.2147/IJN.S26592

Rajput S et al (2015) Overcoming Akt induced therapeutic resistance in breast cancer through siRNA and thymoquinone encapsulated multilamellar gold niosomes. Mol Pharm 12:4214–4225. doi:10.1021/acs.molpharmaceut.5b00692

Ravindran J, Nair HB, Sung B, Prasad S, Tekmal RR, Aggarwal BB (2010) Thymoquinone poly (lactide-co-glycolide) nanoparticles exhibit enhanced anti-proliferative, anti-inflammatory, and chemosensitization potential. Biochem Pharmacol 79:1640–1647. doi:10.1016/j.bcp.2010.01.023

Ryan SM, Brayden DJ (2014) Progress in the delivery of nanoparticle constructs: towards clinical translation. Curr Opin Pharmacol 18:120–128. doi:10.1016/j.coph.2014.09.019

Saad WS, Prud'homme RK (2016) Principles of nanoparticle formation by flash nanoprecipitation. Nano Today. doi:10.1016/j.nantod.2016.04.006

Schneider-Stock R, Fakhoury IH, Zaki AM, El-Baba CO, Gali-Muhtasib HU (2014) Thymoquinone: fifty years of success in the battle against cancer models. Drug Discov Today 19:18–30. doi:10.1016/j.drudis.2013.08.021

Shah M, Naseer MI, Choi MH, Kim MO, Yoon SC (2010) Amphiphilic PHA-mPEG copolymeric nanocontainers for drug delivery: preparation, characterization and in vitro evaluation. Int J Pharm 400:165–175. doi:10.1016/j.ijpharm.2010.08.008

Shah M, Choi MH, Ullah N, Kim MO, Yoon SC (2011) Synthesis and characterization of PHV-block-mPEG diblock copolymer and its formation of amphiphilic nanoparticles for drug delivery. J Nanosci Nanotechnol 11:5702–5710

Shapira A, Livney YD, Broxterman HJ, Assaraf YG (2011) Nanomedicine for targeted cancer therapy: towards the overcoming of drug resistance. Drug Resist Updates 14:150–163. doi:10.1016/j.drup.2011.01.003

Shekunov BY, Chattopadhyay P, Tong HH, Chow AH (2007) Particle size analysis in pharmaceutics: principles, methods and applications. Pharm Res 24:203–227. doi:10.1007/s11095-006-9146-7

Sutton KM, Doucette CD, Hoskin DW (2012) NADPH quinone oxidoreductase 1 mediates breast cancer cell resistance to thymoquinone-induced apoptosis. Biochem Biophys Res Commun 426:421–426. doi:10.1016/j.bbrc.2012.08.111

van Vlerken LE, Amiji MM (2006) Multi-functional polymeric nanoparticles for tumour-targeted drug delivery. Expert Opin Drug Deliv 3:205–216. doi:10.1517/17425247.3.2.205

Woo CC, Loo SY, Gee V, Yap CW, Sethi G, Kumar AP, Tan KH (2011) Anticancer activity of thymoquinone in breast cancer cells: possible involvement of PPAR-gamma pathway. Biochem Pharmacol 82:464–475. doi:10.1016/j.bcp.2011.05.030

Xu S, Olenyuk BZ, Okamoto CT, Hamm-Alvarez SF (2013) Targeting receptor-mediated endocytotic pathways with nanoparticles: rationale and advances. Adv Drug Deliv Rev 65:121–138. doi:10.1016/j.addr.2012.09.041

Zamboni WC et al (2012) Best practices in cancer nanotechnology: perspective from NCI nanotechnology alliance. Clin Cancer Res 18:3229–3241. doi:10.1158/1078-0432.CCR-11-2938

Zeng X, Morgenstern R, Nystrom AM (2014) Nanoparticle-directed sub-cellular localization of doxorubicin and the sensitization breast cancer cells by circumventing GST-mediated drug resistance. Biomaterials 35:1227–1239. doi:10.1016/j.biomaterials.2013.10.042